LETTER

doi:10.1038/nature23014

A novel mechanism for mechanosensory-based rheotaxis in larval zebrafish

Pablo Oteiza[1,2,3]*, Iris Odstrcil[1,2]*, George Lauder[4], Ruben Portugues[3]§ & Florian Engert[1,2]§

When flying or swimming, animals must adjust their own movement to compensate for displacements induced by the flow of the surrounding air or water[1]. These flow-induced displacements can most easily be detected as visual whole-field motion with respect to the animal's frame of reference[2]. Despite this, many aquatic animals consistently orient and swim against oncoming flows (a behaviour known as rheotaxis) even in the absence of visual cues[3,4]. How animals achieve this task, and its underlying sensory basis, is still unknown. Here we show that, in the absence of visual information, larval zebrafish (*Danio rerio*) perform rheotaxis by using flow velocity gradients as navigational cues. We present behavioural data that support a novel algorithm based on such local velocity gradients that fish use to avoid getting dragged by flowing water. Specifically, we show that fish use their mechanosensory lateral line to first sense the curl (or vorticity) of the local velocity vector field to detect the presence of flow and, second, to measure its temporal change after swim bouts to deduce flow direction. These results reveal an elegant navigational strategy based on the sensing of flow velocity gradients and provide a comprehensive behavioural algorithm, also applicable for robotic design, that generalizes to a wide range of animal behaviours in moving fluids.

To describe the behavioural mechanisms of flow navigation in larval zebrafish, we built a system consisting of a horizontal transparent tube in which controlled laminar flow could be induced, and the behaviour of the fish monitored, in three-dimensional space (Fig. 1a–c). We observed that, as previously shown, 5- to 7-day-old larval zebrafish performed rheotaxis by orienting (Fig. 1d, f, g) and swimming (Fig. 1e, h, i) against the direction of the water flow[5]; even in the absence of any visual references[6,7] (Fig. 1f–i).

It is important to point out that under these conditions the flow cannot be directly sensed by the animal if it is being dragged by a homogeneous current. In this scenario, the fish navigates within the reference frame of the constantly moving body of water and all rules of physics are invariant under such a velocity transformation[8]. From the fish's perspective there is no oncoming water flow and, if the flow is truly homogeneous, it is physically impossible to detect it in the absence of cues from an external frame of reference[2,8]. Contact with the wall or linear acceleration detected by the inner ear might provide such cues[9,10]. However, given that fish performed rheotaxis away from the chamber walls (Fig. 1b–c, Extended Data Fig. 1a, b and Supplementary Video 1) and that semicircular canals are not functional in larval stages[11], both touch and angular acceleration were unlikely to play a role in our setup. To test the role of linear acceleration, we mounted the entire behavioural setup on rails, and accelerated it using the same actuator as that for flow induction. We observed no orientation and position-holding behaviour at all acceleration values tested, even at those substantially exceeding the ones used during rheotaxis experiments (Extended Data Fig. 1c–f).

Thus, we hypothesized that the navigational information required for vision–independent rheotaxis had to be provided by border-induced non-homogeneities within the flow. To measure such flow conditions precisely, we used particle image velocimetry (PIV), and observed a radially symmetric flow profile that developed within approximately 5 s and reached steady state thereafter (Fig. 2a and Extended Data Fig. 2a). To investigate the importance of such velocity gradients for flow navigation, we performed experiments across steep, medium, and shallow gradient regimes (Fig. 2b) and observed that the ability of fish to orient and hold position consistently improved with increasing gradient magnitudes (Fig. 2c, d). Trivially, when exposed to a zero-gradient regime, fish did not perform rheotaxis[8] (Fig. 2c, d). Thus, in the absence of visual references, flow velocity gradients represent the main cue for rheotaxis in larval zebrafish.

As any solid body drifting in a fluid containing velocity gradients, a larval zebrafish will experience a rotational flow field (or shear) around its perimeter. The predicted spinning of an object in such a rotational flow field can be observed in the case of a paralysed fish shown in Extended Data Fig. 2b, c and Supplementary Video 2. This rotational flow field is directly related to the local curl of the water volume ($\nabla \times \boldsymbol{V}$) and the two values are mathematically linked by Stokes' theorem, which states that the integrated curl over the area ($\boldsymbol{a}$) occupied by the fish's body (S) can be measured by a line integral around the animal's perimeter:

$$\iint_S (\nabla \times \boldsymbol{V}) \cdot \mathrm{d}\boldsymbol{a} = \oint_C \boldsymbol{V} \cdot \mathrm{d}\boldsymbol{s} \qquad (1)$$

Thus, in our setup, fish could estimate the local curl in the water at its current position by calculating a line integral of the relative water flow around the circumference of its body (Fig. 3a). We will show that the lateral line, a collection of mechanosensory organs distributed along the surface of the body in fish and amphibians[12], is well suited to perform such measurements (the lateral-line integral) and that these measurements provide an elegant and accurate method of estimating local gradient values.

We next focused on the behavioural mechanisms of rheotaxis. Since fish cover a large range of radial distances from the centre of the tube, they experience substantial changes in gradient magnitude during each trial, extending from a flat (zero) gradient at the centre to maximal gradient values close to the border (Figs 2b, 3b, c). As larval zebrafish swim in discrete periods of motor activity (swim bouts)[13] separated by longer inactive inter-bout periods, each swim bout will necessarily elicit a change in the gradient experienced by the fish (delta gradient) that will define the conditions in which the subsequent bout will occur. Thus, during rheotaxis, swim bouts can be grouped into bouts that occur after increases (Fig. 3b–e, red) and bouts that occur after decreases (Fig. 3b–e, blue) in gradient magnitude, where the former generally occur when the fish swims towards the high gradient regime

[1]Department of Molecular and Cellular Biology, Harvard University, Cambridge, Massachusetts 02138, USA. [2]Center for Brain Science, Harvard University, Cambridge, Massachusetts 02138, USA. [3]Max Planck Institute of Neurobiology, Sensorimotor Control Research Group, Martinsried 82152, Germany. [4]Museum of Comparative Zoology, Harvard University, Cambridge, Massachusetts 02138, USA.
*These authors contributed equally to this work.
§These authors jointly supervised this work.

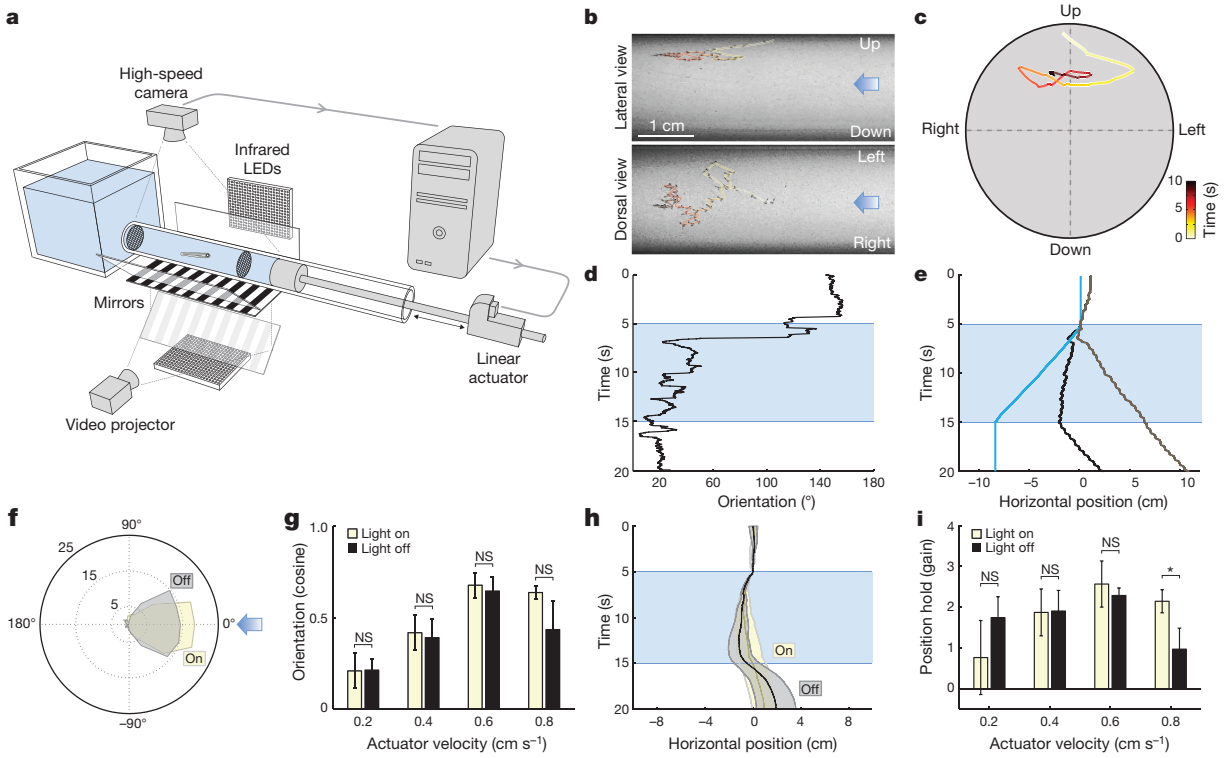

Figure 1 | Larval zebrafish perform rheotaxis in the absence of visual cues. a, Schematics of the setup. **b**, Time-projection of a zebrafish larva performing rheotaxis in the dark. Light blue arrows represent flow direction. **c**, Cross-sectional view of the trial shown in **b**. **d**, **e**, Behavioural features of the trial shown in **b** and **c**. Light blue indicates water flow stimulus is on. **d**, Fish orientation in relation to water flow. **e**, Fish position in the axis of the water flow from the observer's (black trace) and the fish's (grey trace) point of view. Blue trace corresponds to the displacement of the water column. **f**–**i**, Rheotaxis in the presence and absence of visual cues. **f**, Polar plot of fish orientation in the axis of the flow during stimulation. Light blue arrow represents flow direction. **g**, Cosine of the mean orientation (see Methods) for fish presented with different actuator velocities. **h**, Fish position (from the observer's point of view) in the axis of the water flow. **i**, Gain (see Methods) for fish presented with different actuator velocities. $n = 6$ fish subjected to 12 trials at each actuator velocity (288 trials total). Data are shown as means ± s.e.m. NS, $P > 0.05$; $*P > 0.01$ and < 0.05; Monte Carlo permutation test.

of the wall and the latter when it swims away from it. Importantly, we found that while bouts occurring after decreases in gradient magnitude showed a symmetric distribution of low magnitude turns with no obvious directionality (Fig. 3d, blue), the distribution of bouts occurring after increases in gradient magnitude was strongly skewed towards high magnitude turns that followed the direction of the rotational vector field (Fig. 3d, red). These results unveil a simple rheotactic algorithm in which a larval zebrafish, after experiencing a decrease in gradient magnitude, primarily swims straight. On the contrary, after experiencing an increase in gradient magnitude, it performs a high magnitude turn in the direction of flow field rotation (Fig. 3d and Extended Data Fig. 3a). This algorithm relies on small changes in gradient magnitude (Extended Data Fig. 4a–c), occurs mostly in the left–right axis (that is, the yaw) of the fish (Extended Data Fig. 4d–f), is independent of both flow direction (Extended Data Fig. 4g–i) and passive rotations of the animal's body[14] (Extended Data Fig. 2d, e) and, most importantly, allows the fish to both orient and swim against oncoming water flow (Extended Data Fig. 3b–i).

Next, we generated a simple model to test whether our algorithm was sufficient to explain the observed rheotactic behaviour. In this simulation, a particle moved randomly in a virtual flow field that was matched to our experimental conditions (Extended Data Fig. 5a; see Methods). Importantly, we found that this simple algorithm was sufficient to elicit rheotaxis with remarkable robustness (Fig. 3f–g and Supplementary Video 3). In addition, our behavioural experiments also showed that, over the course of a trial, fish swam increasingly closer to the centre of the tube (Extended Data Fig. 6a–c and Supplementary Video 1). This phenomenon, also faithfully reproduced by the model (Extended Data Fig. 6d), is strongly reminiscent of the biased random walk during bacterial chemotaxis[15] and automatically leads to the avoidance of high

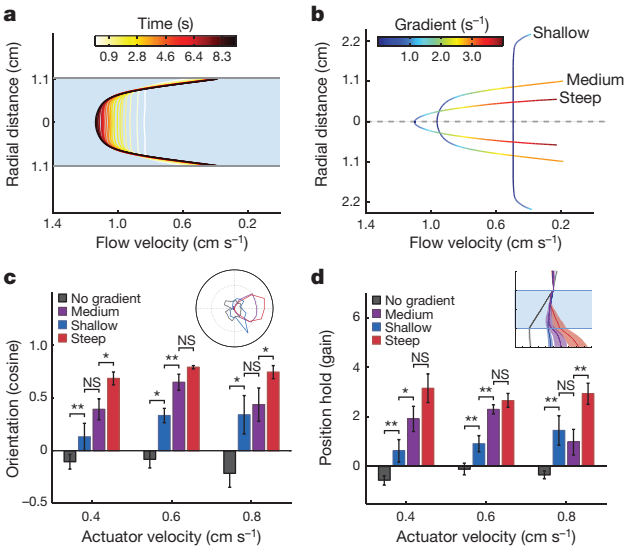

Figure 2 | Flow velocity gradients are the stimulus for rheotaxis in larval zebrafish. a, Development of the flow velocity profile obtained through PIV in the behavioural chamber. **b**, Flow velocity profiles and gradient magnitudes in different diameter tubes (see Methods). **c**, Cosine of the mean orientation for fish presented with different gradient conditions. Inset: polar plot of fish orientation during flow stimulation. **d**, Gain for fish in each of the gradient conditions. Inset: horizontal positions of fish from the observer's point of view. $n = 6$ fish subjected to 6 trials at each actuator velocity (108 trials) for each gradient condition (432 trials total). Medium gradient values are the same as in Fig. 1g, i. Data are shown as means ± s.e.m. NS, $P > 0.05$; $*P > 0.01$ and < 0.05; $**P < 0.01$; Monte Carlo permutation test.

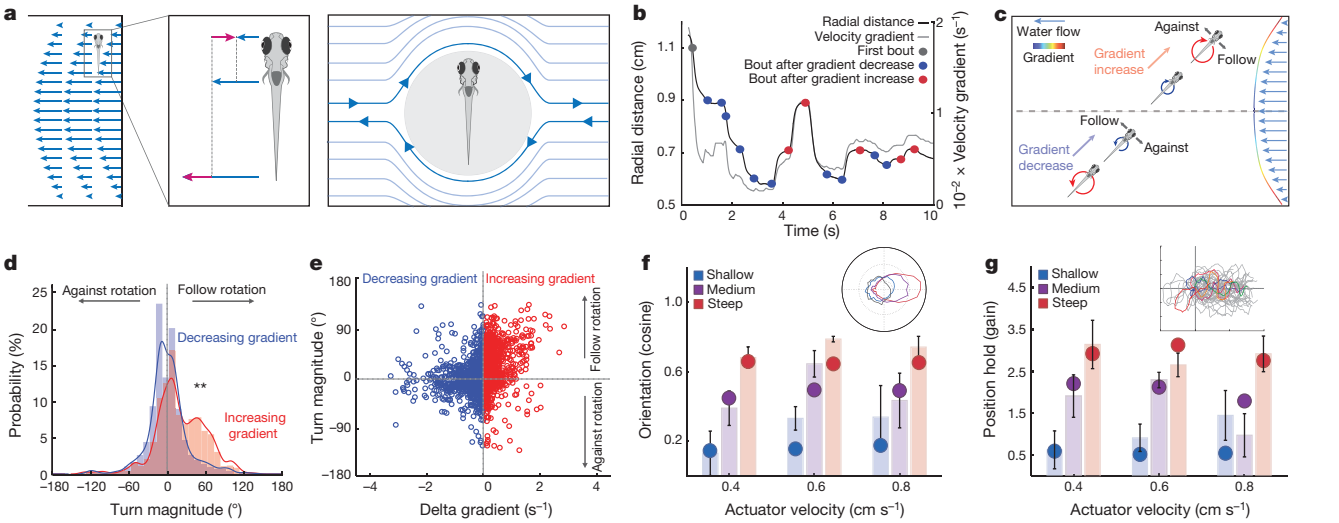

Figure 3 | A behavioural algorithm for rheotaxis in larval zebrafish. **a**, Schematics of gradient-induced rotational flow fields. A fish in a gradient will drift at the flow velocity in its centre of mass (left). Consequently, the differences between fish velocity and the rest of the flow velocities (centre) will induce a local rotational flow field around the animal (right). **b**, Radial distance (grey trace) and velocity gradient (black trace) experienced by a single fish during a trial. Swim bouts occur after increases (red dots) or decreases (blue dots) in gradient magnitude. Data correspond to the example shown in Fig. 1b–e. **c**, Graphical representation of bout types during rheotaxis. **d**, Histogram for turn magnitudes during rheotaxis. $^{**}P < 0.01$. Kolmogorov–Smirnov test, $n = 13$ fish, 341 trials. **e**, Scatter plot of turn magnitude versus delta gradient. $n = 13$ fish, 2,762 bouts. **f**, **g**, Model fish perform rheotaxis. Comparison of cosine of the mean orientation (**f**) and gain (**g**) between model (circles) and real (shaded bars, data as in Fig. 2b, d) fish. Insets: **f**, polar plot of model fish orientation under different gradient conditions; **g**, trajectories of 100 (grey) modelled fish facing a virtual flow towards the left. Five examples are coloured for clarity.

gradient regions near the walls. Interestingly, since high velocity gradients will consistently develop around any obstacles in flowing bodies of water, an algorithm that guides the animal away from a strong gradient will automatically assist in avoiding such obstacles. Somewhat paradoxically, this 'gradient avoidance' effect will eventually lead the fish to veer away from the shore to the centre of the stream, where gradient is lowest and flow velocity is highest. Consequently, we believe that our algorithm selectively applies to animals whose natural habitat is largely restricted to the vicinity of the shore, the reef, or generally to small rivers, brooks, and rivulets, where they are confined to the strong gradients near wall regions[16,17].

Another main feature of natural currents is the presence of turbulence and vortices of varying magnitude. To explore how our proposed algorithm would perform under such disorderly conditions, we added Kármán vortex streets[16–19] to the laminar flow profile used in our simulations (Extended Data Fig. 5a–c). Remarkably, although rheotactic performance invariably decayed with increases in turbulence, it remained consistently robust even when conditions became distinctly unstable (Extended Data Figs 5d–g, 6d and Supplementary Video 3). Interestingly, we also observed that while gain and orientation values depended quite linearly on vortex density (Extended Data Fig. 5f), model performance showed a much more delicate sensitivity to minute changes in vortex intensity (Extended Data Fig. 5g). These extended simulations showed that our algorithm was surprisingly robust to mild and moderate turbulence and could even sustain a minimal baseline performance once fully turbulent flow[19] is established. We propose that the robustness of this effect arises from the consecutive and cumulative integration of many turn angle choices that together average out the random perturbations induced by local vortices.

Finally, we searched for the sensory basis of gradient-dependent rheotaxis. This question, and the role of the lateral line system[12], has been the subject of a continuous debate[3,4,9,10,20]. In the larval zebrafish, the lateral line system consists of a series of mechanosensory organs (the neuromasts) located along multiple stripes in the fish's head (the anterior lateral line) or in single stripes along each side of the fish's tail (the posterior lateral line[21]). To assess its importance in gradient-induced rheotaxis, we performed chemical ablations of all neuromast hair cells using copper sulfate[4,9] (Extended Data Fig. 7a, a′) and observed that turn distributions for bouts occurring after increases or decreases in gradient magnitude almost completely lost their asymmetry (Figs 3d and 4a, b). Consequently, the fish's ability to orient against oncoming water flows was severely reduced (Fig. 4c and Supplementary Video 4). Unilateral and bilateral laser ablations of the anterior or the posterior lateral line nerves (Extended Data Fig. 7b–d′) showed

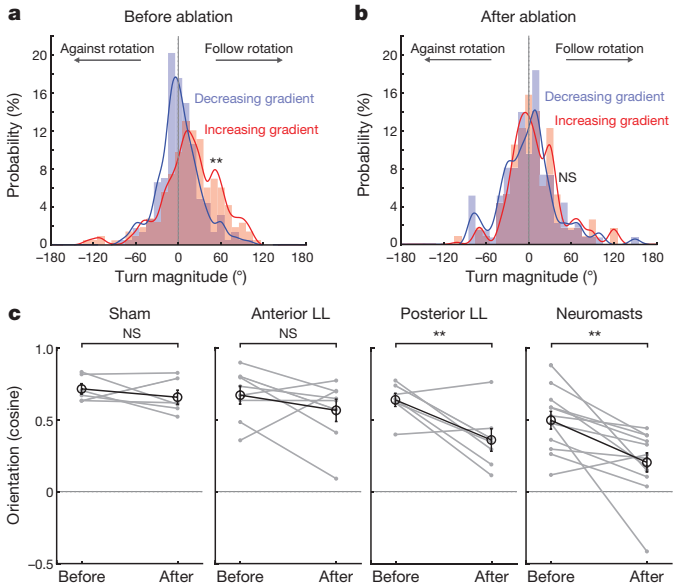

Figure 4 | The mechanosensory lateral line system acts as a gradient sensor during larval zebrafish rheotaxis. **a**, **b**, Turn magnitude histogram before (**a**) and after (**b**) copper-induced chemical ablation of all neuromast hair cells. $^{**}P < 0.01$; Kolmogorov–Smirnov test, $n = 12$ fish. **c**, Mean orientation of fish subjected to different experimental conditions. Mean and s.e.m. of the population (black) and means of individual fish (grey) before and after treatment are shown. *n*: sham, 6 fish; anterior lateral line (LL) ablation, 8 fish; posterior lateral line ablation, 7 fish; chemical neuromast ablation, 12 fish. All fish were subjected to six trials before and after manipulations. NS, $P > 0.05$; $^{**}P < 0.01$; Monte Carlo permutation test.

that the lack of the posterior, but not the anterior, lateral line system induced a significant decrease in the fish's orienting performance (Fig. 4c), which was in agreement with the predominantly left–right component of fish turns during rheotaxis (Extended Data Fig. 4d–f) and the primarily antero-posterior receptive fields of the posterior lateral line neuromasts[22,23]. Furthermore, we found that behavioural loss was comparable in unilaterally as well as bilaterally ablated fish (Extended Data Fig. 7e), suggesting that fish need to integrate the flow over both sides of their body to estimate the curl of local rotational flow fields[24,25].

In summary, our experiments show that a relatively complex behaviour such as rheotaxis can emerge from a surprisingly simple behavioural algorithm that relies on the detection of gradient-induced rotational flow fields. Velocity gradients in natural environments will be present at the interface between flows and any kind of surface; thus the ecological relevance of our algorithm encompasses both rheotaxis as well as obstacle avoidance. Since flow navigation is a fundamental feature of all animals that fly or swim[1], the description of its elementary rules and sensory basis will be essential to unveiling its underlying neural circuits, understanding the evolution of this conserved behaviour, and providing robust algorithms for robot navigation.

Online Content Methods, along with any additional Extended Data display items and Source Data, are available in the online version of the paper; references unique to these sections appear only in the online paper.

Received 16 June 2016; accepted 9 June 2017.
Published online 12 July 2017.

1. Chapman, J. W. *et al.* Animal orientation strategies for movement in flows. *Curr. Biol.* **21,** R861–R870 (2011).
2. Lyon, E. P. On rheotropism I. Rheotropism in fishes. *Am. J. Physiol.* **12,** 149–161 (1904).
3. Dijkgraaf, S. The functioning and significance of the lateral-line organs. *Biol. Rev. Camb. Phil. Soc.* **38,** 51–105 (1963).
4. Montgomery, J., Baker, C. F. & Carton, A. G. The lateral line can mediate rheotaxis in fish. *Nature* **389,** 960–963 (1997).
5. Olszewski, J., Haehnel, M., Taguchi, M. & Liao, J. C. Zebrafish larvae exhibit rheotaxis and can escape a continuous suction source using their lateral line. *PLoS ONE* **7,** e36661 (2012).
6. Suli, A., Watson, G. M., Rubel, E. W. & Raible, D. W. Rheotaxis in larval zebrafish is mediated by lateral line mechanosensory hair cells. *PLoS ONE* **7,** e29727 (2012).
7. Olive, R. *et al.* Rheotaxis of larval zebrafish: behavioral study of a multi-sensory process. *Front. Syst. Neurosci.* **10,** 14 (2016).
8. Galilei, G. *Dialogo sopra i due massimi sistemi del mondo* (transl. Drake, S.) (Univ. California Press, 1967).
9. Van Trump, W. J. & McHenry, M. J. The lateral line system is not necessary for rheotaxis in the Mexican blind cavefish (*Astyanax fasciatus*). *Integr. Comp. Biol.* **53,** 799–809 (2013).
10. Arnold, G. P. Rheotropism in fishes. *Biol. Rev. Camb. Phil. Soc.* **49,** 515–576 (1974).
11. Beck, J. C., Gilland, E., Tank, D. W. & Baker, R. Quantifying the ontogeny of optokinetic and vestibuloocular behaviors in zebrafish, medaka, and goldfish. *J. Neurophysiol.* **92,** 3546–3561 (2004).
12. Münz, H. in *The Mechanosensory Lateral Line: Neurobiology and Evolution* (eds Coombs, S., Gorner, P. & Münz, H.) 285–298 (Springer, 1989).
13. Budick, S. A. & O'Malley, D. M. Locomotor repertoire of the larval zebrafish: swimming, turning and prey capture. *J. Exp. Biol.* **203,** 2565–2579 (2000).
14. Yuan, J., Raizen, D. M. & Bau, H. H. Propensity of undulatory swimmers, such as worms, to go against the flow. *Proc. Natl Acad. Sci. USA* **112,** 3606–3611 (2015).
15. Berg, H. *Random Walks in Biology* (Princeton Univ. Press, 1993).
16. von Kármán, T. Mechanische Ähnlichkeit und Turbulenz. *Nachr. Ges. Wiss. Gottingen Math.-Phys. Kl.* **5,** 58–76 (1930).
17. Carlson, R. L. & Lauder, G. V. Escaping the flow: boundary layer use by the darter *Etheostoma tetrazonum* (Percidae) during benthic station holding. *J. Exp. Biol.* **214,** 1181–1193 (2011).
18. Tritton, D. J. *Physical Fluid Dynamics* 2nd edn, 18–25, 277 (Clarendon, 1988).
19. Barkley, D. *et al.* The rise of fully turbulent flow. *Nature* **526,** 550–553 (2015).
20. Hofer, B. Studien über die Hautsinnesorgane der Fische. I. Die Funktion der Seitenorgane bei den Fischen. *Ber. Kgl. Bayer. Biol. Versuchsstation München* **1,** 115–164 (1908).
21. Ghysen, A. & Dambly-Chaudière, C. Development of the zebrafish lateral line. *Curr. Opin. Neurobiol.* **14,** 67–73 (2004).
22. López-Schier, H., Starr, C. J., Kappler, J. A., Kollmar, R. & Hudspeth, A. J. Directional cell migration establishes the axes of planar polarity in the posterior lateral-line organ of the zebrafish. *Dev. Cell* **7,** 401–412 (2004).
23. Nagiel, A., Andor-Ardó, D. & Hudspeth, A. J. Specificity of afferent synapses onto plane-polarized hair cells in the posterior lateral line of the zebrafish. *J. Neurosci.* **28,** 8442–8453 (2008).
24. Ristroph, L., Liao, J. C. & Zhang, J. Lateral line layout correlates with the differential hydrodynamic pressure on swimming fish. *Phys. Rev. Lett.* **114,** 018102 (2015).
25. Hildebrand, D. G. C. *et al.* Whole-brain serial-section electron microscopy in larval zebrafish. *Nature* **545,** 345–349 (2017).

Supplementary Information is available in the online version of the paper.

Acknowledgements We are grateful to E. Soucy and J. Greenwood for technical support, and B. Jordan for discussions. We thank M. Baldwin, M. Häsemeyer, and T. Dunn for reading the manuscript, and M. McHenry for advice on the behavioural rig. We also thank M. Grünthal and R. Hellmiss for contributions to figure design, and V. Stih for sharing unpublished data. This work was supported by a Pew Latin-American Fellowship to P.O., BRAIN National Institutes of Health (NIH) grant U01NS090449, NIH Pioneer award, and DP1 NS082121 to F.E., Simons Foundations grant SCGB 325207 and Human Frontier Science Program grant RGP0033/2014 to F.E., and an Office of Naval Research grant N00014-09-1-0352 to G.L., monitored by T. McKenna. R.P. was funded by the Max-Planck-Gesellschaft during part of this work.

Author Contributions P.O. conceived the project, built the rig, performed the experiments, and analysed the data. P.O, I.O., and F.E. designed the experiments. I.O. performed the chemical and two-photon lateral line ablations. P.O. and R.P. designed the software for the behavioural rig. P.O. and G.L. performed the PIV experiments. R.P., F.E., and I.O. contributed to the mathematical and theoretical considerations. I.O. and F.E. wrote the model. P.O., I.O., and F.E. wrote the manuscript with the assistance of R.P. and G.L. All authors discussed the data and the manuscript.

Author Information Reprints and permissions information is available at www.nature.com/reprints. The authors declare no competing financial interests. Readers are welcome to comment on the online version of the paper. Publisher's note: Springer Nature remains neutral with regard to jurisdictional claims in published maps and institutional affiliations. Correspondence and requests for materials should be addressed to P.O. (mijaelsmith@googlemail.com), R.P. (rportugues@neuro.mpg.de) or F.E. (florian@mcb.harvard.edu).

Reviewer Information *Nature* thanks E. Brainerd, J. Dabiri and the other anonymous reviewer(s) for their contribution to the peer review of this work.

METHODS

Animals. Five to seven days post-fertilization (d.p.f.), wild-type zebrafish of the WIK strain were used for all behavioural experiments, unless indicated. Animal handling and experimental procedures were approved by the Harvard University Standing Committee on the Use of Animals in Research and Training. No statistical methods were used to predetermine sample size. The experiments were not randomized. The investigators were not blinded to allocation during experiments and outcome assessment.

Behavioural chamber. A 45-cm-long polycarbonate tube (1.27, 2.22, or 4.76 cm inner diameter, 0.31 cm wall thickness) was attached to a water reservoir and filled with aquarium water. Two 140 μm mesh filters were used to contain single zebrafish larvae in a 13-cm-long behavioural section while two infrared light-emitting diode arrays provided illumination from below and from the sides of the tube. A high-speed camera (Pike F-032B, Allied Vision Technologies) fitted with a macro-lens (Sigma DG, USA) and a visible-light-blocking filter (to block visual cues in light-on experiments) recorded fish behaviour at 200 frames per second directly from above the behavioural section and from the reflection of a lateral infrared reflecting mirror (hot mirror, Edmund Optics, USA). For experiments in which visual cues were present, stationary black and white stripes (0.5 cm wide) from a mini-projector (Dell M109S, USA) were reflected upwards on a visible light-reflecting mirror (cold mirror, Edmund Optics, USA) into a diffusive screen underneath the behavioural section. Laminar water flow was created by the displacement of a custom-made plunger attached to the rod of a computer-controlled linear actuator (Servotube Actuator STA1112, Copley Controls). For acceleration and water displacement experiments, the behavioural section of the rig was mounted on rails and attached to the actuator's rod. Behavioural trials were controlled using software custom-written in LabView (National Instruments, Austin, Texas, USA) and consisted of 5 s of no stimulus, 0.1 s acceleration, 9.8 s water flow/water displacement stimulus, 0.1 s de-acceleration, and another 5 s of no stimulus. For acceleration experiments, trials consisted of 2.5 s of no stimulus, 1 s of acceleration, 1 s of water displacement, 1 s of de-acceleration, and another 2.5 s of no stimulus. All experiments were performed by randomly moving the plunger towards or away from the water reservoir.

Behavioural analysis. All behavioural analyses used custom-written MATLAB code (MathWorks). Rheotactic orientation was calculated as the mean of the cosines of all fish orientations during stimulus presentation. Thus, cosine = 1 represented perfect alignment against flow direction (0° fish orientation) while cosine = −1 represented perfect alignment in the direction of the flow (180° fish orientation). To quantify the ability to hold position against incoming flows, we calculated a relation between the velocity of the fish and the velocity of the incoming water flow (the 'gain') through the formula (fish velocity minus water velocity)/water velocity. Thus, gain < 1 meant fish actively swim in the direction of the flow, gain = 0 represented passive drift, gain = 1 meant perfect position holding, and gain > 1 meant overcompensation. This metric was used for individual bout types (that is, Extended Data Fig. 3i) or, by calculating their mean, for a whole behavioural trial (that is, Fig. 1i). Since flow stimulus onset and direction were always randomized, both cosine and whole-trial gain were calculated from a similar number of experiments in which the fish faced towards or against the direction of the flow at the beginning of the stimulus. For paralysed fish experiments, larval zebrafish were incubated in 1 mg ml^{-1} of α-bungarotoxin and then directly released into the behavioural chamber while water flow was induced. Except for minor necessary modifications (that is, swimming versus paralysed fish), all analyses used the same code, independently of the experiment type.

Statistics. Kolmogorov–Smirnoff tests were performed through embedded functions while Monte Carlo permutation tests were custom written in MATLAB (MathWorks). For the latter, we calculated the difference between the means of the two distributions to be compared; then both distributions were shuffled and a new difference in means was calculated. This was repeated through 10,000 iterations and the *P* value was calculated as the probability of finding the original difference of the means. No variance analyses were performed.

Water flow analysis. PIV was performed as previously described[26]. Water velocity profiles were calculated at 50 frames per second (Davis software version 7.2.2, LaVision, Goettingen, Germany) and analysed using custom software written in MATLAB (MathWorks). Different flow profiles were created by the displacement of actuator-attached plugs into small (1.27 cm), medium (2.22 cm), and large (4.76 cm) diameter polycarbonate tubes. For behavioural analyses, flow stimulus direction was always taken as leftwards and all the time points (except for the initial acceleration) during flow development were used. As the average horizontal position of the fish during rheotaxis was 6.5 ± 0.7 cm away from the flow source (either the plunger or the water reservoir), behavioural analyses were performed using the flow profile obtained at 5–7 cm away from the source (Fig. 2a and Extended Data Fig. 2a). All time points in the development of the flow profile were matched to the time points in the behavioural videos. Since both flow profile and rheotactic behaviour between experiments in which the flow was induced towards or away from the water reservoir were similar (Supplementary Fig. 4g–i), all trials were included in the analyses.

Modelling. Modelling of the rheotactic algorithm was made using software custom-written in LabView (National Instruments, Austin, Texas, USA). In brief, our simulations consisted of a particle randomly moving in a virtual flow field that matched our experimental conditions with the following constraints: the path-length of each iterative step corresponded to the average bout distance travelled by a larval zebrafish, the time taken for each step was set to the average bout frequency, and turn angles were drawn from the distributions described in Fig. 3d. Finally, delta gradient values were obtained by the change in position of the particle within the measured flow field described in Fig. 2a. Additionally, under high velocity conditions, the fixed bout length of the model fish was gradually upregulated during a successful trial to account for similar observations under experimental conditions (data not shown). To add turbulence to the model, we equipped our simulation platform with the ability to add Kármán vortex streets to the laminar flow profile described in Extended Data Fig. 5. The maximum value (100%) of the rotational speed of each individual vortex (intensity) was set to the maximal absolute velocity of the parabolic velocity profile of the stream. The vortex density was defined by the relative spacing of hexagonally arranged vortices with respect to each other.

Lateral line ablations. For chemical neuromast ablations, 5–7 d.p.f. WIK larvae were used. Fish were subjected to six trials at a single actuator velocity (0.6 cm s^{-1}), incubated in 1 mM copper sulfate for 85 min and allowed to rest in fish water for 60 min before being subjected to six more trials. Only fish that showed a complete neuromast ablation (assessed by DiASP staining[27]) and a constant swimming activity were included in the analysis. For two-photon lateral line nerve ablations, 6 d.p.f. *HGn93D* zebrafish larvae[28] were subjected to six trials at a single actuator velocity (0.6 cm s^{-1}) and embedded in low-melting-point agarose with one of their otic vesicles looking upwards. An image stack of the green fluorescent protein (GFP)-labelled lateral line nerve in the *HGn93D* strain was acquired and then one to three 850 nm laser pulses of 1 ms duration were targeted on the anterior or the posterior central projection of the lateral line nerve. For sham ablations, the same treatment was performed on a single neighbouring nerve innervating a dorsal neuromast. Fish were then released from the agarose and rested for 24 h to allow the regeneration of the neuromast cupula after being damaged during agarose release. In the case of bilateral lateral line ablations, fish were immediately mounted and ablated on their opposite side after being released from the agarose and allowed to rest for 24 h. The next day, fish were subjected to another six trials, re-embedded in agarose, and another stack of the lateral line nerve was acquired. Only fish with normal buoyancy, constant swim activity, and with clear damage to the lateral line nerve targeted in the treatment were included in the analysis. All experiments were analysed using the same code, independently of the ablation type.

Data availability. All codes and video data that support the findings of this study are available from the corresponding authors upon request.

26. Drucker, E. G. & Lauder, G. V. Locomotor forces on a swimming fish: three-dimensional vortex wake dynamics quantified using digital particle image velocimetry. *J. Exp. Biol.* **202,** 2393–2412 (1999).
27. Schuster, K. & Ghysen, A. Labeling second-order sensory neurons in the posterior lateral-line system of zebrafish. *Cold Spring Harb. Protoc.* **2013,** 1175–1177 (2013).
28. Pujol-Martí, J. *et al.* Neuronal birth order identifies a dimorphic sensorineural map. *J. Neurosci.* **32,** 2976–2987 (2012).

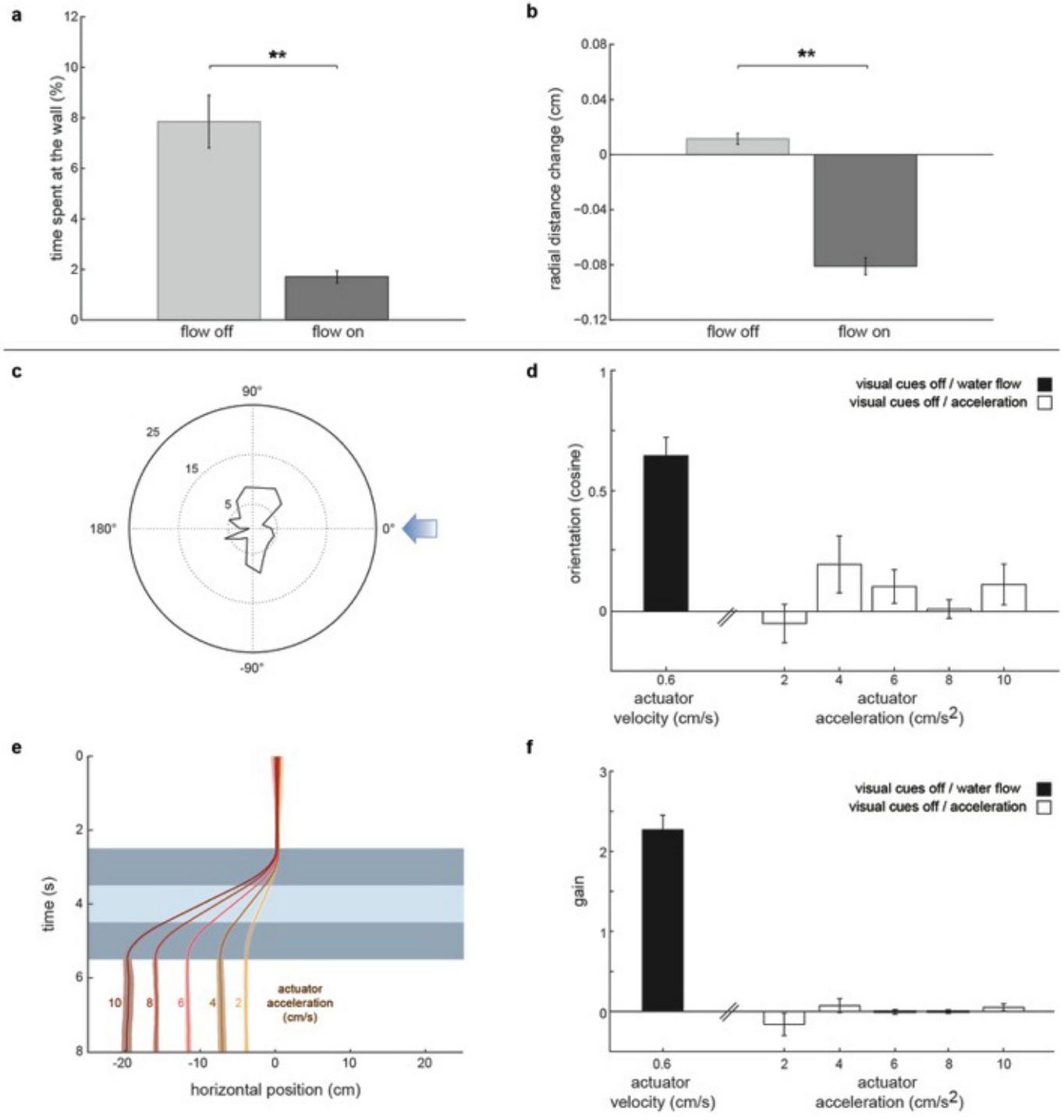

Extended Data Figure 1 | Touch and acceleration do not explain rheotaxis in larval zebrafish. a, Percentage of time fish spend at the wall. $n = 13$ fish, 341 trials. **b**, Mean radial distance change for bouts occurring in close proximity to the wall (<0.36 cm, one-third of the tube radius). $n = 13$ fish, 1,364 bouts. **c**–**f**, Rheotactic metrics for larval zebrafish exposed to a series of acceleration/water displacement/de-acceleration stimuli. **c**, Polar plot of fish orientation in the axis of the stimulation. Blue arrow represents stimulus direction. **d**, Cosine of the mean orientation for fish presented with different acceleration regimes. Black bar represents cosine of the mean orientation for fish exposed to water flow in the dark (Fig. 1g). **e**, Fish position (from the observer's point of view) in the axis of the stimulus. Dark blue represents acceleration/de-acceleration periods; light blue represents water displacement. **f**, Gain for fish presented with different acceleration regimes. Black bar represents gain for fish exposed to water flow in the dark (Fig. 1i). $n = 6$ fish subjected to 6 trials at each acceleration regime (180 trials total). All data are shown as means ± s.e.m. $^{**}P < 0.01$; Monte Carlo permutation test.

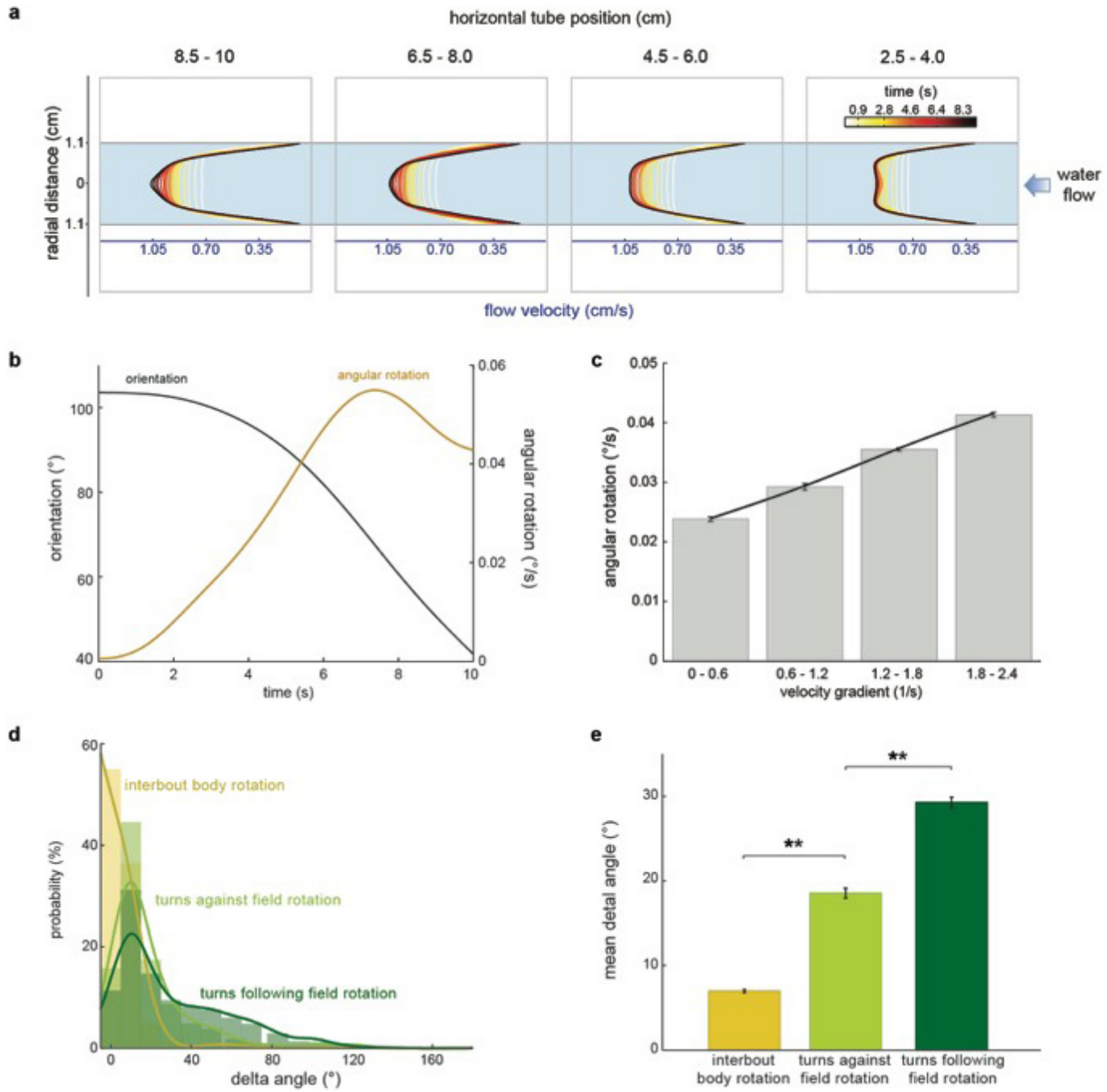

Extended Data Figure 2 | Gradient-dependent rotation of the larval zebrafish body. a, Development of flow velocity profiles obtained through PIV at different points in the horizontal axis of the tube (see Methods). **b**, Orientation (black) and angular rotation (brown) changes in a single paralysed larval zebrafish in water flow. Data correspond to the example shown in Supplementary Video 2. **c**, Mean angular rotational velocities for different velocity gradient magnitudes. $n = 3$ fish, 18 trials. **d**, Inter-bout body rotation (yellow) and turn magnitude histogram for bouts going against (light green) and following (dark green) flow rotational fields. Histograms and fitted lines for each distribution are shown. $n = 13$ fish, 341 trials. **e**, Mean delta angle for inter-bout body rotation and turns following/going against flow field rotation. $n = 3{,}840$ inter-bout periods, 2,831 bouts. Means and ± s.e.m. (**c**, **e**) and bars and fitted lines (**d**) are shown. $^{**}P < 0.01$; Monte Carlo permutation test.

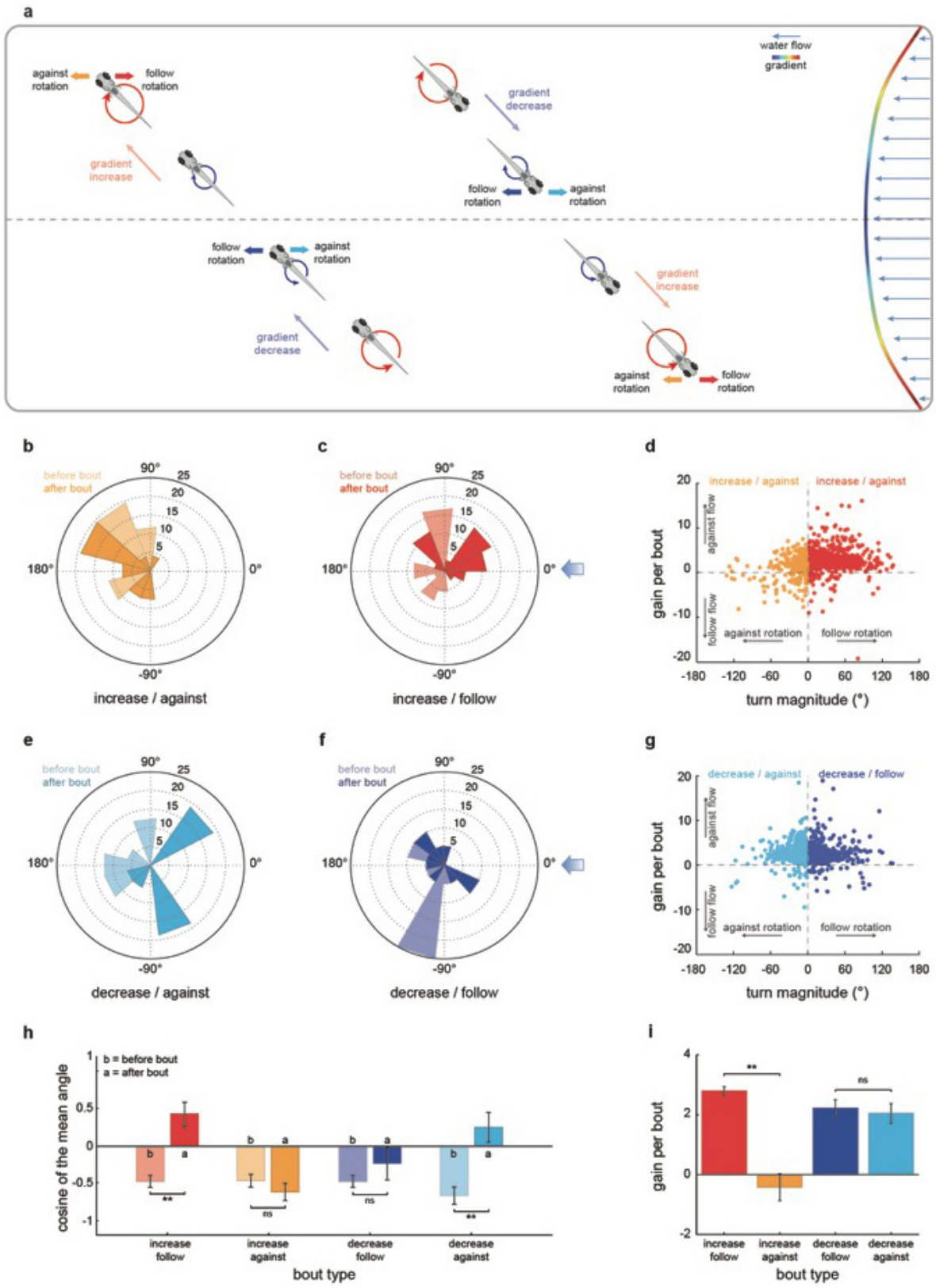

Extended Data Figure 3 | The rheotactic algorithm allows the fish to orient and swim against incoming water flows. a, Graphical representation of bout types during rheotaxis. **b**, **c**, **e**, **f**, Polar plots of fish orientation before (light colour) and after (dark colour) high magnitude (>45°) turns that start when fish is facing away from the flow. $n = 98$ bouts. **d**, **g**, Scatter plots of turn magnitude versus gain for bouts occurring after increases (**d**) or decreases (**g**) in gradient magnitude. $n = 2{,}598$ bouts. **h**, Cosine of the mean orientation for the data shown in **b**, **c**, **e** and **f**. **i**, Gain for high magnitude turns extracted from the data shown in **d** and **g**. $n = 508$ bouts. Data are shown as means ± s.e.m. $^{*}P > 0.01$ and < 0.05; $^{**}P < 0.01$, Monte Carlo permutation test.

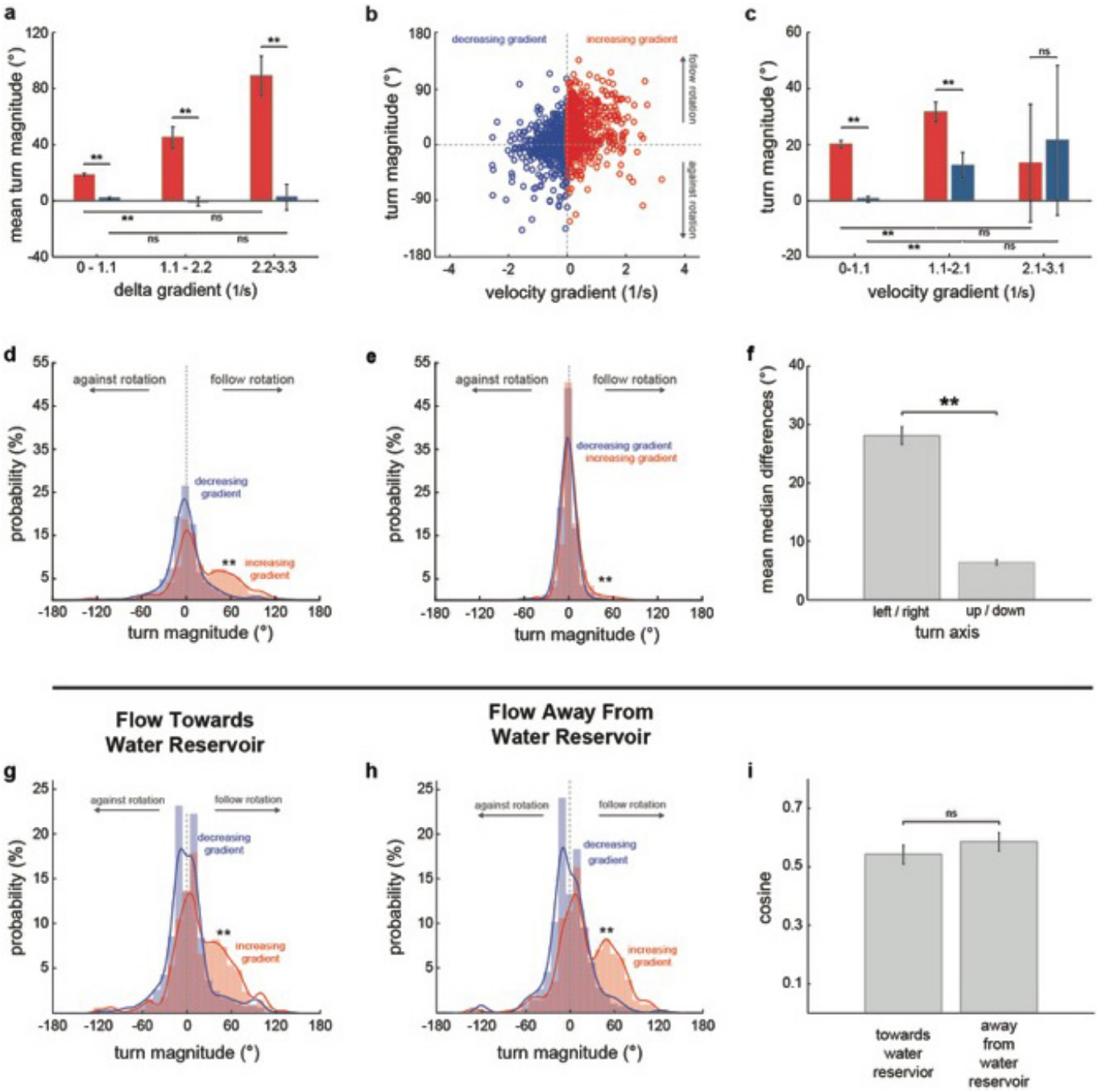

Extended Data Figure 4 | The rheotactic algorithm depends on delta velocity gradients, is mainly composed of lateral turns, and is independent of flow direction. a, Mean turn magnitude for bouts occurring after increases or decreases in gradient magnitude, grouped by delta gradient. Data are the same as in Fig. 3e. **b**, Scatter plot of absolute velocity gradient versus turn magnitude for bouts occurring at intermediate tube regions (0.36–0.74 cm away from the walls) that could be reached from both low and high gradient areas. $n = 13$ fish, 1691 bouts. **c**, Mean turn magnitude for bouts after increases or decreases in gradient magnitude, grouped by absolute velocity gradient. Data are the same as in **b**. **d**, **e**, Turn magnitude histogram for left/right (**d**) and up/down (**e**) turns. $n = 13$ fish, 341 trials. **f**, Mean difference between the medians of increasing and decreasing gradient turn distributions. Data are the same as in **d** and **e**. **g**–**i**, Turn magnitude histogram for experiments in which water flowed towards (**g**) or away from (**h**) the water reservoir. $n = 13$ fish; 170 and 171 trials for flow towards and flow away from experiments, respectively. **i**, Cosine of the mean orientation for flow towards and flow away from experiments. Data are the same as in **g** and **h**. Means and ± s.e.m. (**a**, **c**, **f**, **i**) and bars and fitted lines (**d**, **e**, **g**, **h**) are shown. NS, $P > 0.05$; $^{**}P < 0.01$; Kolmogorov–Smirnov (**d**, **e**, **g**, **h**) and Monte Carlo permutation (**a**, **c**, **f**, **i**) tests.

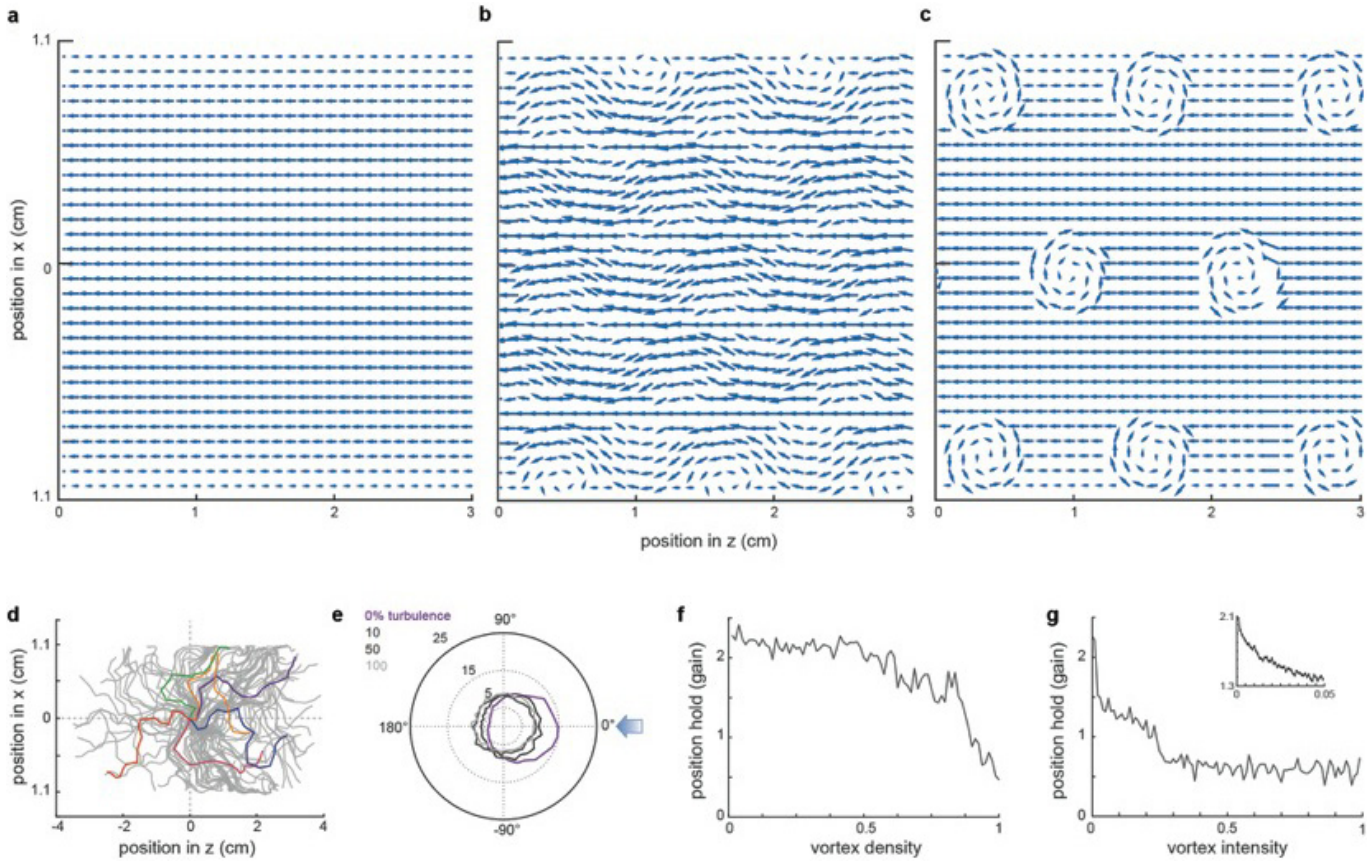

Extended Data Figure 5 | Model fish perform rheotaxis in a virtual turbulent flow. a, Virtual laminar flow profile used for modelling rheotactic behaviour (Fig. 3f, g). **b**, Flow profile in **a** after the addition of Kármán vortex streets to **a** at 50% intensity and 100% density. **c**, Flow profile in **a** after the addition of static vortices set to 100% intensity and 100% density. **d**, Trajectories of 100 (grey) modelled fish facing a virtual turbulent flow towards the left. Five examples are coloured for clarity. **e**, Polar plot of model fish orientation under different turbulence strengths. **f**, Gain of model fish as a function of increasing vortex density at a constant 100% vortex intensity. **g**, Gain of model fish as a function of increasing vortex intensity at a constant 100% vortex density. Inset is an expanded view of the initial gain drop.

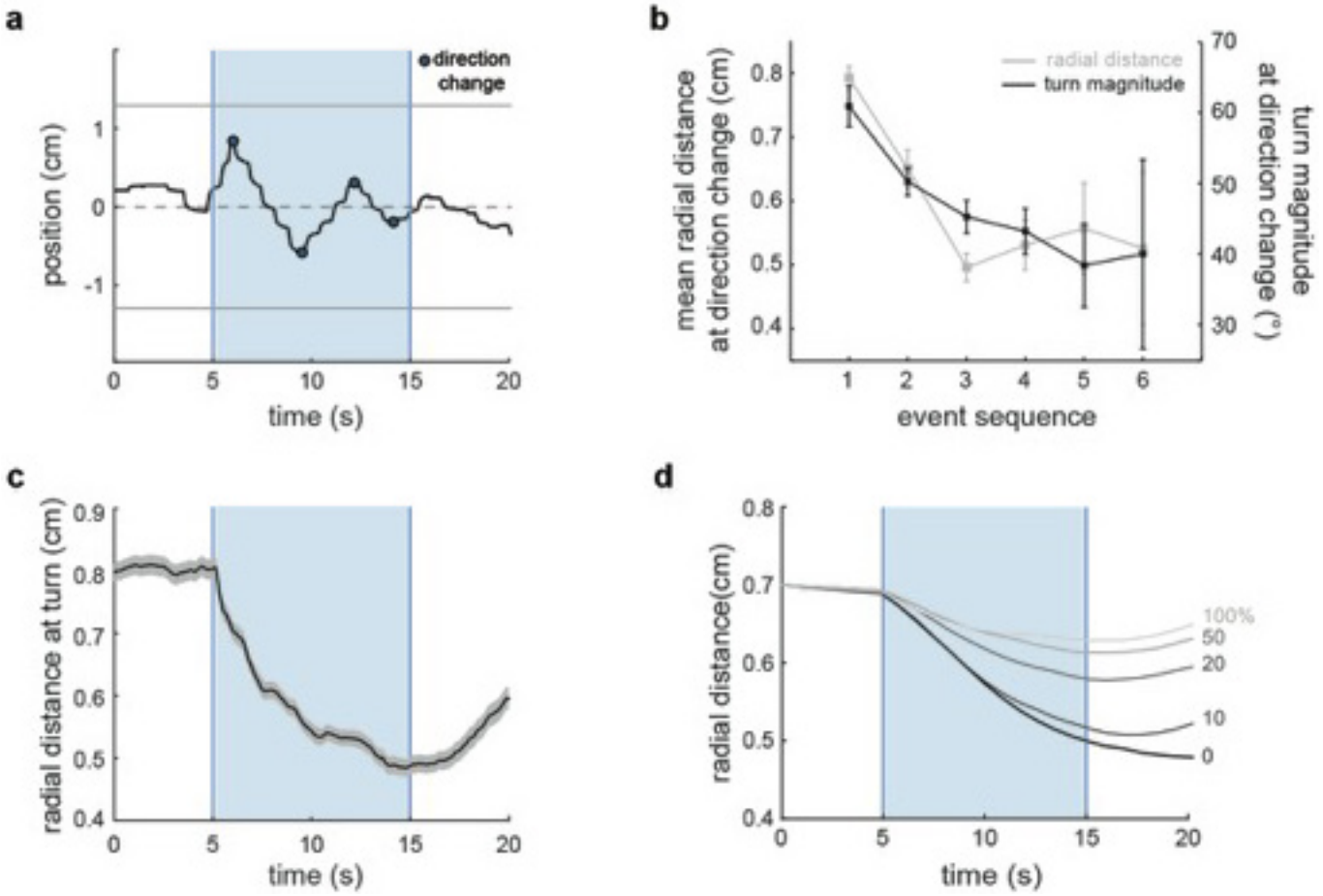

Extended Data Figure 6 | Larval zebrafish swims towards the centre of the tube during rheotaxis. a, Horizontal (left/right) positions of a single fish during rheotaxis. Light blue indicates water flow stimulus; dark blue dots indicate direction change events. Data correspond to the example shown in Fig. 1b–e. **b**, Radial distance and turn magnitude at consecutive swim direction changes. $n = 774$ direction change events. **c**, Radial distance over time. $n = 13$ fish, 341 trials. **d**, Radial distance over time for a modelled particle following the rheotactic algorithm at different vortex densities. Data are shown as means ± s.e.m. $^{**}P < 0.01$; Monte Carlo permutation test.

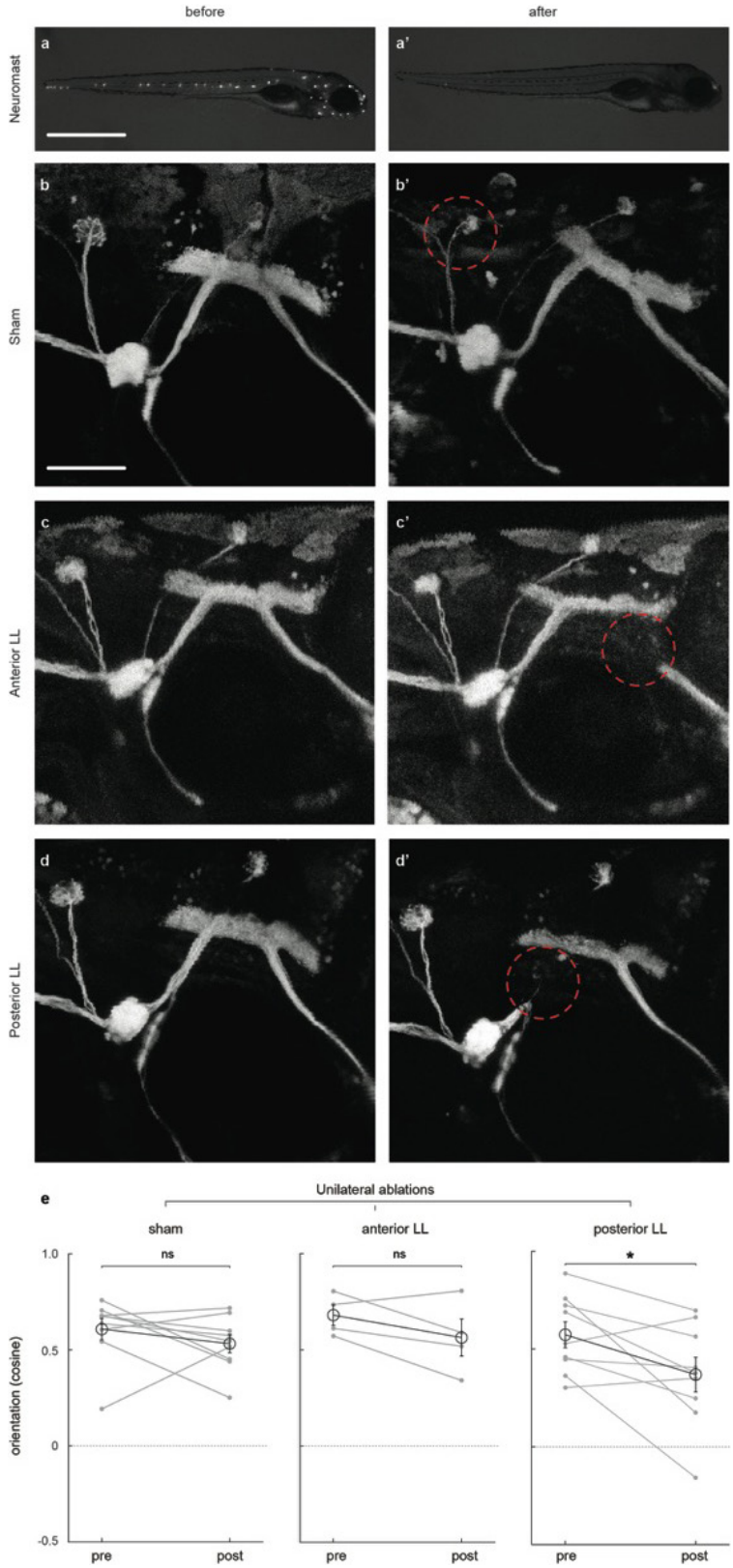

Extended Data Figure 7 | Bilateral lateral line stimulation is required for rheotaxis in larval zebrafish. a–d′, Representative examples of copper-mediated chemical neuromast (**a**, **a′**) and two-photon laser sham (**b**, **b′**), anterior (**c**, **c′**), and posterior (**d**, **d′**) lateral line nerve ablations before (left column) and after (right column) treatment. DiasP-stained (**a**, **a′**) and GFP-expressing Tg(HGn93D) fish shown. Red dotted circles indicate the region in which laser power was focused. **e**, Cosine of the mean orientation for fish subjected to unilateral laser ablations of the lateral line nerve. Mean and s.e.m. of the population (black) and means of individual fish (grey) before and after treatment are shown; *n*: sham, 9 fish; anterior lateral line ablation, 4 fish; posterior lateral line ablation, 9 fish. All fish were subjected to six trials before and after manipulations. NS, $P > 0.05$; $^*P < 0.05$ and > 0.01; Monte Carlo permutation test.

doi:10.1038/nature23096

BIOMECHANICS

How fish feel the flow

Hair-like sensors are suspected to aid fish navigation in complex environments. Laboratory experiments and computational simulations reveal how these sensors can detect water flow to direct the swimming responses of fish.

JOHN O. DABIRI

It's hard out there for a fish. Survival requires constant vigilance to avoid predators and obstacles, especially in near-shore environments. Although many fish exploit visual cues to escape harm, the greatest danger that lurks in the water is largely invisible: the persistent and unpredictable churning of currents, which can carry an unsuspecting fish far off course or cause it to crash into underwater objects. Moreover, some fish are naturally blind or live in light-poor regions where visual cues are minimal. Yet even under such circumstances, fish are remarkably effective at maintaining a constant position at the same location (a phenomenon known as station-keeping) and avoiding obstacles.

These feats have been attributed to the action of motion-sensitive hair cells that form a structure called the lateral line, which runs along the length of a fish's body[1,2]. But how does the lateral line sense local patterns of water motion, and how do fish use that information to navigate? In a paper online in *Nature*, Oteiza *et al.*[3] propose an elegant mechanism based on a robust principle of fluid dynamics, which only requires the fish to respond to the flow by making a simple choice between either continuing to swim without changing direction or making a turning manoeuvre.

Oteiza and colleagues conducted laboratory experiments in which larval zebrafish (*Danio rerio*) swam in a transparent cylindrical tube through which water was pumped at a steady speed. Friction between the water and the walls of the tube slows the water at the sides, creating a spatial gradient in the speed of the flow from the centre of the cylinder, where the flow is fastest, to the stationary water that is in contact with the tube walls.

The authors confirmed that, consistent with previous studies[4–6], the zebrafish could position themselves in the tube away from the walls and orient their bodies to swim against the direction of water flow (Fig. 1). Because both skills come in handy for station-keeping and obstacle avoidance in nature, the laboratory experiments provide a useful system with which to mimic and investigate swimming processes that are relevant to life in the wild. By performing chemical ablations of the lateral line and conducting experiments in the dark to remove visual cues, the researchers demonstrated that the lateral-line system was necessary to achieve oriented movement in response to water flow (a process known as rheotaxis), and that this orientation could not be based on touch or sensing the uniform acceleration of the surrounding mass of water.

How does the lateral line help a fish to orient itself? Oteiza and colleagues' key insight is the application of a nineteenth-century mathematical theorem named after physicists William Thomson (Lord Kelvin) and George Stokes[7]. The Kelvin–Stokes theorem states that, in most cases, the local flow gradients in any region of a fluid will be uniquely associated with the velocity of the flow along a closed loop that surrounds the region. In other words, if a swimming fish can combine knowledge of the speed of the flow of water along different parts of its body — a task enabled by the machinery that the lateral-line system provides — then the information it gathers is sufficient to deduce local gradients in flow speed. The gradients relevant to the Kelvin–Stokes theorem in this context are related to the tendency of the local fluid to rotate, a property known as its vorticity.

One way to understand the connection between flow gradients and fluid rotation is to imagine a boat positioned with its bow

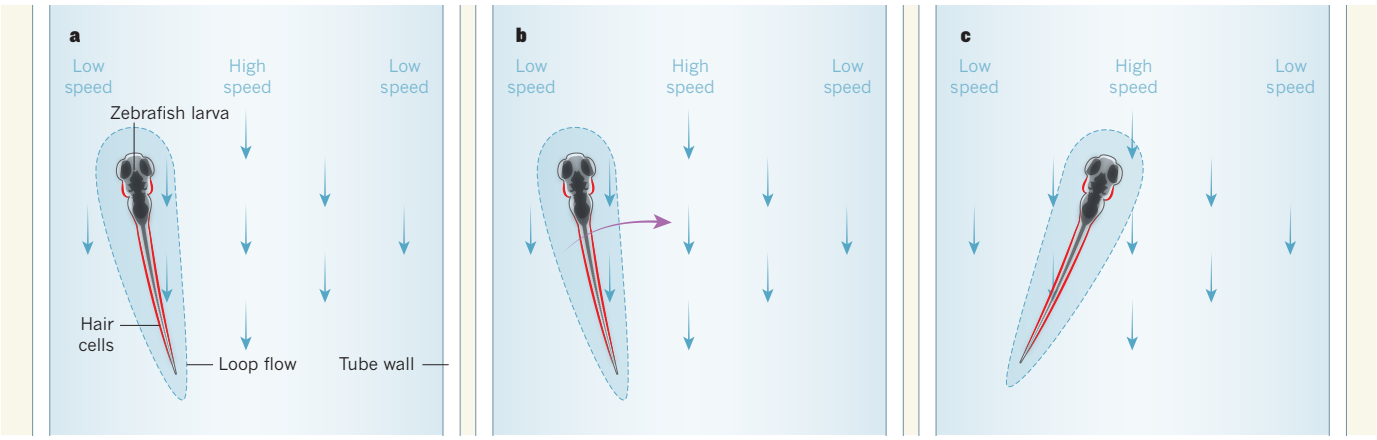

Figure 1 | Flow-based navigation. **a**, To understand how fish adjust their position when swimming, Oteiza *et al.*[3] studied the response of larval zebrafish (*Danio rerio*) in a tube in which water moves at high speed at the centre and at low speed near the walls. Blue arrows indicate the direction of the water flow. Zebrafish have a series of hair cells (location of cells shown in red) known as the lateral line, and the authors propose that this system can sense the flow of water in a loop (dashed blue line) that surrounds the fish. They demonstrate that the Kelvin–Stokes theorem[7] can be used to translate the sensed fluid flow into knowledge of the tendency of the fluid inside the loop to rotate (a phenomenon known as vorticity), as well as the magnitude of the corresponding flow-speed gradients, and that sensing these aspects of fluid flow can help to guide fish navigation. **b**, Oteiza and colleagues observed that when a fish swims towards a region of increasing difference between the flow speeds on either side of its body, the fish turns (purple arrow) in the same direction as the local rotation of the water (not shown), which is also the direction that will carry the fish away from obstacles. **c**, Navigation that is based on the lateral-line sensing of flow-speed gradients enables the fish to swim at the centre of the tube and to avoid the walls. In the wild, this ability could enable fish to navigate complex underwater environments in which visual cues might be insufficient.

facing the direction of the water flow, with water flowing past the boat's right-hand side faster than on its left. If the boat were floating passively, when viewed from above, it would begin to rotate clockwise. The speed of this rotation would be proportional to the difference in the flow speeds on either side, which form a gradient across the boat. A similar information pathway — sensing the velocity around the fish's body through the lateral line, followed by deducing the corresponding direction of local vorticity and estimating the local flow-speed gradients, which are proportional to the vorticity — is at the heart of the proposed mechanism for flow-based navigation in zebrafish.

Successful navigation requires a way of using knowledge of local flow conditions to robustly guide a fish away from harm. The researchers made a striking observation in relation to this. Whenever a fish swam towards a region in which the difference between the flow speeds on either side of its body increased in comparison to the difference at the fish's previous location, the fish made a turn in the direction of the local flow vorticity (by veering either clockwise or anticlockwise). This action reliably steered the animal away from the region near the wall, and towards the centre of the oncoming flow. Conversely, when the fish swam towards a region in which the flow gradients decreased in comparison to those it encountered previously, it continued to swim in the same direction without a turning bias. Because flow gradients usually decrease the farther away a fish is from a solid object, this navigation strategy should translate into the avoidance of real-world obstacles and the bodies of predators.

The authors took important first steps towards extending their results beyond the realm of controlled laboratory experiments by developing computer simulations that demonstrated the robustness of their observations when modelling the situation in quasi-turbulent flows. However, real aquatic environments present other challenges, such as 3D flow that cannot be navigated solely with turns in a horizontal plane. In addition, the Kelvin–Stokes theorem that underlies the proposed navigation strategy can fail if there are local sources or sinks of water in the vicinity, such as the suction flow that some predators use to ingest prey[4]. Paradoxically, the proposed mechanism for rheotaxis could also lead fish towards regions of flow that, although they exhibit small flow gradients, could simultaneously have large, uniform flow speeds that overpower the fish's ability to escape such strong currents. Thus, the mechanism described by Oteiza and colleagues is probably paired with other sensing strategies — yet to be discovered, and perhaps also making use of the lateral line — that enable fish to navigate the full complexity of the underwater world. As the full repertoire of these sensing and control skills becomes apparent, we will not only learn more about fish ecology, but might also gain inspiration for new types of bio-robotic navigation in both water and air. ■

John O. Dabiri *is in the School of Engineering, Stanford University, Stanford, California 94305, USA.*
e-mail: jodabiri@stanford.edu

1. Dijkgraaf, S. *Biol. Rev. Camb. Phil.* **38,** 51–105 (1963).
2. Montgomery, J. C., Baker, C. F. & Carton, A. G. *Nature* **389,** 960–963 (1997).
3. Oteiza, P., Odstrcil, I., Lauder, G., Portugues, R. & Engert, F. *Nature* http://dx.doi.org/10.1038/nature23014 (2017).
4. Olszewski, J., Haehnel, M., Taguchi, M. & Liao, J. C. *PLoS ONE* **7,** e36661 (2012).
5. Suli, A., Watson, G. M., Rubel, E. W. & Raible, D. W. *PLoS ONE* **7,** e29727 (2012).
6. Olive, R. *et al. Front. Syst. Neurosci.* **10,** 14 (2016).
7. Saffman, P. G. *Vortex Dynamics* (Cambridge Univ. Press, 1992).